Ollscoil na Gaillimhe
University of Galway

Provided by the author(s) and University of Galway in accordance with publisher policies. Please cite the published version when available.

Title	A multistage selective weighting method for improved microwave breast tomography
Author(s)	Shahzad, Atif; O'Halloran, Martin; Jones, Edward; Glavin, Martin
Publication Date	2016-08-24
Publication Information	Shahzad, Atif, O'Halloran, Martin, Jones, Edward, & Glavin, Martin. (2016). A multistage selective weighting method for improved microwave breast tomography. Computerized Medical Imaging and Graphics, 54, 6-15. doi: http://dx.doi.org/10.1016/j.compmedimag.2016.08.007
Publisher	Elsevier
Link to publisher's version	http://dx.doi.org/10.1016/j.compmedimag.2016.08.007
Item record	http://hdl.handle.net/10379/6343
DOI	http://dx.doi.org/10.1016/j.compmedimag.2016.08.007

Downloaded 2024-04-26T22:52:11Z

Some rights reserved. For more information, please see the item record link above.

A Multistage Selective Weighting Method for Improved Microwave Breast Tomography

Atif Shahzad[1, *], Martin O'Halloran[1], Edward Jones[1], Martin Glavin[1]

[1] *Electrical and Electrnics Enginnering, National University of Ireland Galway, Ireland*

Abstract

Microwave tomography has shown potential to successfully reconstruct the dielectric properties of the human breast, thereby providing an alternative to other imaging modalities used in breast imaging applications. Considering the costly forward solution and complex iterative algorithms, computational complexity becomes a major bottleneck in practical applications of microwave tomography. In addition, the natural tendency of microwave inversion algorithms to reward high contrast breast tissue boundaries, such as the skin-adipose interface, usually leads to a very slow reconstruction of the internal tissue structure of human breast. This paper presents a multistage selective weighting method to improve the reconstruction quality of breast dielectric properties and minimize the computational cost of microwave breast tomography. In the proposed two stage approach, the skin layer is approximated using scaled microwave measurements in the first pass of the inversion algorithm; a numerical skin model is then constructed based on the estimated skin layer and the assumed dielectric properties of the skin tissue. In the second stage of the algorithm, the skin model is used as *a priori* information to reconstruct the internal tissue structure of the breast using a set of temporal scaling functions. The proposed method is evaluated on MRI-derived breast phantoms and a comparison with the standard single-stage technique is presented.

Keywords: `Medical Imaging`, `Microwave Tomography`, `Breast Imaging`

*Corresponding author

2010 MSC: , 92C55, 78A46, 78M20, 78A70

1. Introduction

Microwave imaging has been extensively investigated for a range of applications, particularly in the areas of medical imaging, subsurface imaging, nondestructive testing of materials, and detection of cracks in materials. One of the most notable applications is microwave breast imaging, where a number of clinical prototypes have already been developed and reported in recent literature [1, 2, 3, 4]. Microwave imaging can be generally classified into two categories: a radar based approach [5, 6, 7, 8] that constructs images based on energy scattered from abnormalities in the breast; while a second technique called microwave tomography [9, 10, 11, 12, 13, 14], reconstructs the full spatial distribution of dielectric properties of the breast tissues using inverse scattering algorithms. The radar based approach is computationally simple, but the reconstructed images can only be used to locate strong microwave scatterers in the imaging space, providing scatterer shape and size information. Therefore, the radar based approach can be more appropriate in applications that aim to localize abnormalities in the breast. Conversely, microwave tomography has the potential to reconstruct the entire dielectric profile of the breast that can be directly mapped to different tissue types in the breast. However, it comes at much higher computational cost compared to radar based techniques. Recent developments in digital computing and the availability of fast parallel tomography solutions such as [15] have supported the development of microwave tomography as one of the major alternatives for breast imaging. The microwave inverse problem is nonlinear and inherently ill-posed. Therefore, it requires numerical treatment such as regularization or linearization to achieve an optimal solution. Linear approximation methods, such as the Born and Rytov approximations are used in [16, 17, 18] and found to be effective for imaging objects with low dielectric contrast, but they fail to reconstruct dielectric profiles with higher contrast and larger objects [19]. Therefore, the linearized methods are restricted to only

qualitative image reconstruction, where the location and shape of abnormalities in the breast can be imaged. Several nonlinear iterative algorithms such as [10, 11, 20] have been developed to reconstruct the quantitative dielectric profile of the breast. The computational cost of these algorithms primarily depends on the choice of forward solution and the additional processing involved in the stabilization of the inversion method. The forward solution and the stabilization techniques are often strongly associated with the inversion algorithms. Therefore, the obvious solution to minimize the computational cost is to reduce the number of iterative steps by improving the convergence rate, and enhancing the throughput of computational hardware. In breast imaging applications, the dielectric contrast between skin and healthy breast tissue (mostly adipose) under the skin is quite high [21], which results in strong reflections from the skin layer even in the presence of an appropriate matching liquid. The amount of energy that penetrates through the skin-adipose interface is considerably lower than the reflected energy, and the relative amplitude of skin reflections in the measured electromagnetic (EM) signals is significantly higher than the reflections from the internal tissue structures of the breast. As a result, skin reflections in the measured EM signals dominate the behavior of the objective function in the minimization problem. Therefore, the iterative inversion algorithms tend to reward the high dielectric contrast of the skin-adipose layer, and fail to accurately reconstruct the internal tissue structure of the breast. In addition, convergence of the reconstruction process is severely affected by the masking effect of the skin layer, resulting in extremely slow reconstruction of the dielectric properties of the internal tissue structures of breast. This paper presents an iterative multistage inversion technique to improve the convergence rate and the reconstruction quality of dielectric profile of the human breast. A selective scaling approach is applied to estimate the skin layer in the first stage (Stage I), and the internal structure of the breast is reconstructed in the second stage (Stage II) using selective spatial and temporal scaling functions. The estimated skin layer is assigned approximate dielectric properties based on the measurements available in [22], and used as *a priori* information in the second stage. The proposed

Multistage Selective Weighting Method (MSWM) is verified using simulated microwave data from a set of MRI derived numerical breast phantoms [23], and a comparison with a standard time domain microwave inversion method is presented. The remainder of the paper is organized as follows: Section 2 describes the microwave inversion algorithm and the challenges in breast imaging application. Section 3 presents the multistage inversion technique and selective weighting approach. Section 4 presents the results of numerical simulations and discussion. The conclusion and future work are presented in Section 5.

2. Microwave Inversion Algorithm

In the microwave inversion algorithm, the error between measured EM signals from the target object and the computed EM signals from an estimated numerical model of the target is minimized using either a frequency domain formulation [2, 12, 24, 18, 25] or a time domain formulation [20, 10]. In the frequency domain formulation, single frequency measurements are generally used to reconstruct the target profile, which simplifies the inverse problem but proves inadequate for reconstructing highly heterogeneous human breast tissue. The solution can be improved by including more data, which can be done by either increasing the number of spatial samples (number of illuminations) or frequency samples (multi-frequency illumination). The former of these solutions is bounded by the physical geometry of the breast and antenna coupling effects, while the latter is practically feasible by acquiring multi-frequency measurements on the target imaging domain. Several multi-frequency solutions, such as [2, 26, 27], have been introduced to improve the reconstruction quality and stability of the frequency domain inversion algorithms. However, the complexity of these algorithms significantly increases with the use of multi-frequency data. Conversely, time domain inversion algorithms benefit from the use of wideband excitation signals, but are affected by the dispersive nature of biological tissue, which affects all multi-frequency approaches. In recent studies, it has been shown that the use of wideband measurements has improved the solution of

the microwave inverse problem [2]. Therefore, an ultra wideband Time Domain Inversion Scattering (TDIS) algorithm based on [10] is considered in this study. Various studies, such as [28, 29, 30] have demonstrated the efficacy of the TDIS in recovering the dielectric properties of breast tissue using simulated numerical data. The TDIS method has been extended in [20, 31] to recover parameters of a Debye model that can be applied to dispersive medium, such as human tissue. More recently, the computational throughput of TDIS has been improved by introducing a massively parallel execution model for breast imaging applications [15]. However, the effect of the skin-adipose contrast has largely been ignored under the assumption that the skin information is known *a priori*, and in most of the numerical models, the skin layer is either ignored or used as an estimate in the inversion process. In this paper, the effects of the skin-adipose boundary on the inverse solution are studied, and a multistage solution to reconstruct the dielectric properties of the breast is proposed, assuming that the skin information is unknown. Although the computational time in reconstructing the dielectric profile of breast has been reduced, it is still impractical for real time application to reconstruct 3D (three dimensional) profile through UWB time domain inversion method. Considering the extremely high computational complexity of 3D inversion algorithms, this paper focuses only on the 2D formulation, and extends the work presented in [15]. The 2D formulation presented in this paper is straight forward to extend to a 3D reconstruction problem.

2.1. Formulation of Time Domain Inversion

Consider an array of M antennas placed around a breast of unknown dielectric properties as shown in Fig. 1(a). A set of $M \times N$ measurements is recorded where each antenna transmits, and scattered electromagnetic signals are measured on N receiving antennas, where $N < M$. Another set of $M \times N$ measurements is recorded from an assumed numerical model of the breast, using estimated dielectric properties. The least square solution to the minimization

problem can be expressed as:

$$F(u) = \int_0^T \Big[\sum_{m=1}^{M} \sum_{n=1}^{N} |E_{m,n}^{meas}(t) - E_{m,n}^{est}(u,t)|^2 \Big] dt + \alpha \int_V \|\nabla u\|^2 dV \quad (1)$$

where $E_{m,n}^{meas}(t)$ and $E_{m,n}^{est}(u,t)$ are the measured and estimated electrical signals at receiving antenna n corresponding to a transmitted pulse from antenna m. $u = (u_1, u_2, ..)$ are the parameters of model describing the frequency dependent permittivity of material. It is assumed that the material is non-magnetic. $t \in [0, T]$, where T is the measurement time; M and N are the number of the transmitting and receiving points, respectively. The second term in equation 1 is introduced to enforce Tikhonov regularization [32], where α is the regularisation parameter. The derivative of the objective function $F(u)$ can be estimated by first order perturbation, where the dielectric parameters u are perturbed by a factor δ in the direction u', such that $u \to u + \delta u'$. Thus, the Fréchet differential of the objective function using adjoint principle, can be derived from:

$$\delta F'(u) = \langle G_u, \delta u \rangle \quad (2)$$

where G_u is the gradient w.r.t. u, and inner product $\langle , \rangle$ is defines over the estimation region S as:

$$\langle a, b \rangle = \iint_S a(r) b(r) dS \quad (3)$$

The gradients with respect to each parameter of the dispersion model can be represented as sum of the inner products of unknown parameters:

$$\delta F'(u) = \sum_i \langle g_i, \delta u_i \rangle \quad (4)$$

2.1.1. Dielectric Dispersion model

The frequency dependence of dielectric permittivity can be modelled using a single pole Debye model, as used in [20, 31]. The frequency dependent complex permittivity of the discretized volume of the target can be described as:

$$\epsilon(\omega, r) = \epsilon_0 \big[\epsilon_\infty(r) + \frac{\epsilon_{static}(r) - \epsilon_\infty(r)}{1 + j\omega\tau(r)} \big] + \frac{\sigma(r)}{j\omega} \quad (5)$$

where $\epsilon_\infty(r)$ and $\epsilon_{static}(r)$ are the permittivity values at highest and lowest frequencies in spectrum, respectively. $\sigma(r)$ is conductivity, $\tau(r)$ is the relaxation constant, ω is radial frequency, and $r = (x, y)$ is discretised spatial position. The relaxation $\tau(r)$ can be considered constant for first order, and a single variable $\Delta\epsilon$ can be introduced to model variation in permittivity over complete frequency range, where $\Delta\epsilon(r) = \epsilon_{static}(r) - \epsilon_\infty(r)$. Therefore, the unknown parameter vector u can be defined as:

$$u = (u_1, u_2, u_3) = (\epsilon_\infty, \Delta\epsilon, \sigma) \tag{6}$$

By expanding the equation 4 , the gradients w.r.t each unknown parameter can be derived as:

$$g_{u_1}(r) = 2\int_0^T \left[\sum_{m=1}^{M}\left(E^{adj}_{m,r}(u,t) \odot \frac{d}{dt}E^{est}_{m,r}(u,t)\right)\right]dt + \alpha.\nabla^2 u_1(r) \tag{7a}$$

$$g_{u_2}(r) = -2\int_0^T \left[\sum_{m=1}^{M}\left(P^{adj}_{m,r}(u,t) \odot E^{est}_{m,r}(u,t)\right)\right]dt + \alpha.\nabla^2 u_2(r) \tag{7b}$$

$$g_{u_3}(r) = 2\int_0^T \left[\sum_{m=1}^{M}\left(E^{adj}_{m,r}(u,t) \odot E^{est}_{m,r}(u,t)\right)\right]dt + \alpha.\nabla^2 u_3(r) \tag{7c}$$

where $E^{est}_{m,r}(u,t)$ is the (numerically) estimated EM field at spatial position r in the reconstruction space due to a transmitter m, over an assumed numerical model of the problem domain. $E^{adj}_{m,r}(u,t)$ is the adjoint solution to Maxwells field equations. The symbol $\odot$ represents an element-wise product of two vectors. $P^{adj}_{m,r}(u,t)$ is the polarization density, estimated through numerical adjoint solution, which is calculated by reverse time propagation of the difference signals from all the receiving antennas back to transmitting antenna m. The difference signals are calculated as:

$$E^{diff}_{m,n}(t) = [E^{meas}_{m,n}(t) - E^{est}_{m,n}(u,t)] \tag{8}$$

The gradients are used in the conjugate gradient method to find the conjugate direction, and the optimal step size α is determined by a line search in the conjugate direction. The dielectric parameters in the k^{th} iteration are updated

at each spatial position as:

$$u_i^{k+1}(r) = u_i^k(r) + \alpha^k d_i^k(r), \qquad i = 1, 2, 3 \tag{9}$$

where conjugate directions $d_i^k(r)$ are determined using the Polak-Ribire (PR) method [33]. The complete inversion algorithm is presented in Table 1.

Table 1: Microwave Inversion Algorithm

1.	Start with initial guess, u_0
2.	For $k = 1, 2, 3, .., n$ to convergence
3.	Calculate (numerically) $E_{m,r}^{est}(u,t)$, $E_{m,r}^{adj}(u,t)$, and $P_{m,r}^{adj}(u,t)$
5.	Calculate gradients $g_{u_i}^k$: eqn. 7
6.	Update conjugate directions: β is the PR parameter $d_{u_i}^{k+1} = -g_{u_i}^k + \beta_{u_i}^k d_{u_i}^k,$ i=1,2,3
7.	Find step size by line search: minimize $arg \underset{\alpha}{min}\ F(u^k + \alpha d^k)$
8.	Update parameter vector: $u_i^{k+1} = u_i^k + \alpha^k d_i^k,$ i=1,2,3
9.	Test convergence criteria: κ is a predefined threshold $\lvert F(u^k) - F(u^0)\rvert / \lvert F(u^0)\rvert < \kappa$

2.2. Challanges in Microwave Breast Imaging

Previous studies examining the dielectric properties of human breast tissue [21, 34] have shown the heterogeneity of breast tissues and high contrast between skin tissue and healthy breast tissues (mostly adipose) under the skin layer. Electromagnetic scattering relies on the contrast, where the scattered energy is directly proportional to the dielectric contrast between the two layers of tissue. In practical imaging systems, a coupling liquid with matched dielectric properties is typically used to minimize the reflections from the skin-background interface [35]. However, there is always an unavoidable reflection from the skin-adipose interface due to the high dielectric contrast between skin and adipose

tissue. The effect of this high contrast interface on the measured EM signals can be observed in Fig. 1 where the simulated EM field at different time instances is shown to highlight the reflections from the two skin-adipose interfaces (I_1 & I_2).

A large portion of the transmitted signal is reflected from the skin-adipose interface (I_1) and a relatively small amount of EM energy penetrates through the interface to the interior of the breast. Similarly on the second interface (I_2), the energy that penetrates through the interface to the outside of the breast is much lower than the energy reflected from the scatterers within the breast. Therefore, the measured energy from internal tissue structures at the receiving antennas is significantly smaller than any direct path signals and the skin reflections. In addition, multiple reflections within the region contained by the skin layer interact with the scattered EM signals, resulting in additional clutter in the measured signals. The EM field gradients are estimated with respect to dielectric parameters using the reciprocity principle with the adjoint EM field. The high dielectric contrast at the skin-adipose layer combined with relatively larger magnitudes of total EM fields at the skin-adipose interface, results in large gradients at the skin layer, as shown in Fig. 2. A simplified numerical breast phantom is used to show the effect of higher contrast at skin-adipose layer. The Debye parameters for the breast phantom are derived from [23], and shown in Fig. 2 (A-C) for reference. Fig. 2 (D) shows the real part of the permittivity at centre frequency (4GHz) of the broadband pulse used in simulations. The gradient with respect to ϵ_∞ is shown in Fig. 2 (E). Although the dielectric contrast of the scatterer (modeled as a tumor) within the healthy breast tissue (modeled as adipose) is much larger than the contrast of skin with adipose, the relative magnitude in the gradient is significantly smaller compared to the skin. As a result, the skin layer is rewarded in the reconstruction process and the tomography algorithm naturally exhibits a bias towards the skin compared to other tissues deeper in the breast. Meaney *et al.* [11] introduced a log-magnitude and unwrapped phase transformation technique in the frequency domain inversion method to recover the properties of high

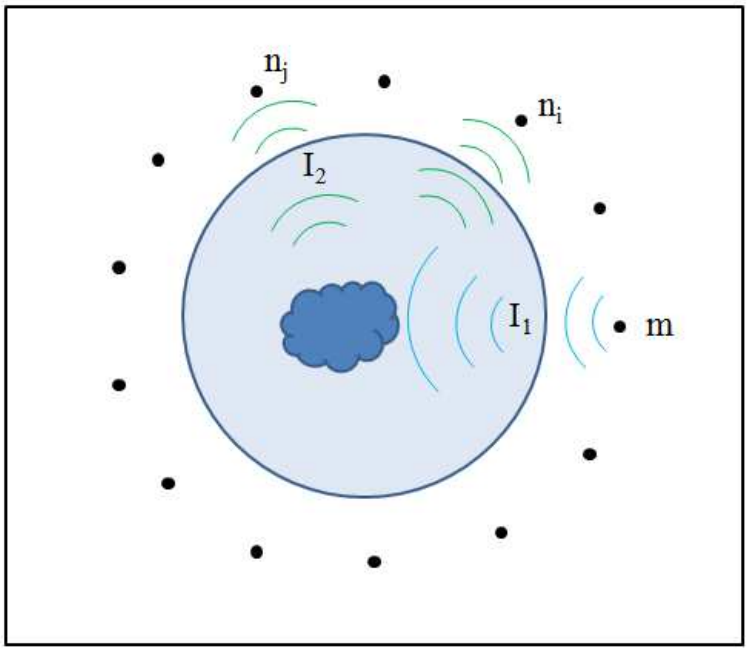

(a) Simplified breast model with circular antenna array, showing two skin-adipose interfaces.

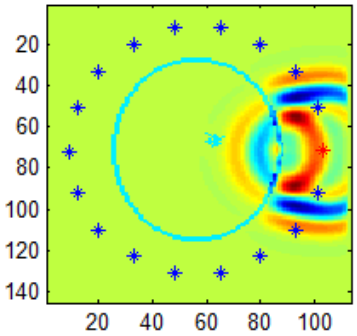

(b) Simulated scattered energy map showing reflections from skin-adipose interface I_1.

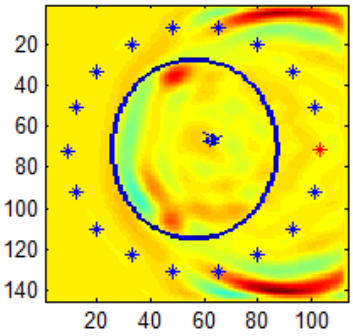

(c) Simulated scattered energy map showing reflections from skin-adipose interface I_2.

Figure 1: Skin Effects: a comparison of the amount of energy reflected and penetrated through the skin-adipose interface. The transmitting antennas are highlighted in red and the reflections from two interfaces (I_1 and I_2) are shown in (b) and (c). The labels on vertical and horizontal axis show span in millimeters.

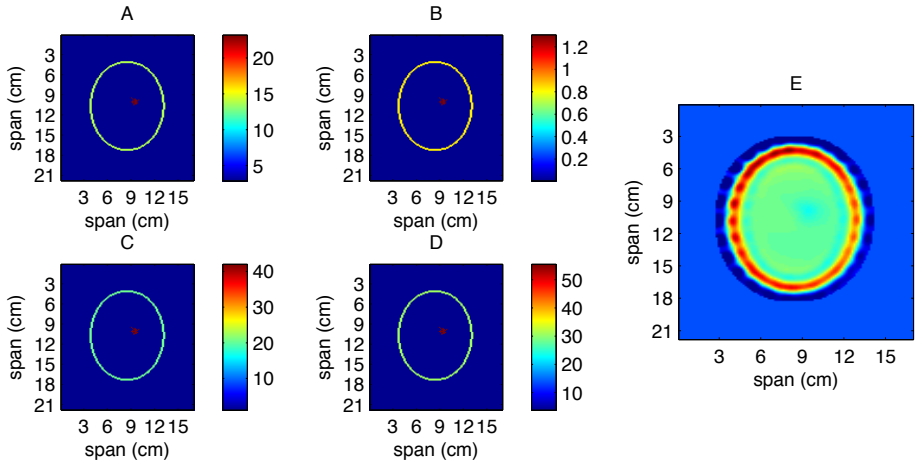

Figure 2: Skin Effects: Debye model parameters ϵ_∞, σ, and $\Delta\epsilon$ of a simplified numerical breast phantom are shown in (A), (B) and (C). Real part of the permittivity at 4GHz is shown in (D), and the gradient with respect to ϵ_∞ is shown in (E).

contrast objects. It can also reduce the influence of high contrast skin-adipose interface on the reconstruction quality.

However in TDIS, the reconstruction quality and the convergence rate can be significantly improved by using skin information (location and dielectric properties) in the reconstruction process. A multistage solution with a selective weighting approach is presented in the following section.

3. Multistage Selective Weighting Approach

3.1. Parameter Scaling

Considering the higher sensitivity of tomography algorithms to the high contrast and the lossy nature of biological tissues, a novel spatial scaling technique is introduced in this paper. The EM field gradients are calculated using pre-scaled EM signals, according to:

$$g_{u_1}(r) = \int_0^T \Bigg[\sum_{m=1}^{M} \gamma(r,m) \Bigg(E^{adj}_{m,r}(u,t) \odot \frac{d}{dt} E^{est}_{m,r}(u,t) \Bigg) \Bigg] dt + \alpha . \nabla^2 u_1(r) \quad (10a)$$

$$g_{u_2}(r) = - \int_0^T \Bigg[\sum_{m=1}^{M} \gamma(r,m) . \Bigg(P^{adj}_{m,r}(u,t) \odot E^{est}_{m,r}(u,t) \Bigg) \Bigg] dt + \alpha . \nabla^2 u_2(r) \quad (10b)$$

$$g_{u_3}(r) = \int_0^T \Bigg[\sum_{m=1}^{M} \gamma(r,m) . \Bigg(E^{adj}_{m,r}(u,t) \odot E^{est}_{m,r}(u,t) \Bigg) \Bigg] dt + \alpha . \nabla^2 u_3(r) \quad (10c)$$

where the spatial scaling function $\gamma(r,m) = 2.e^{(\frac{2\pi . \bar{\sigma} ||r-m||}{\lambda . \sqrt{\bar{\epsilon}}})}, for \quad i = 1,2,3$ is pre-computed for each transmitter m and the spatial location r in the reconstruction grid, resulting in an $M \times R$ matrix. Here, M is the number of transmitters, R is the number of discretized spatial points in the reconstruction grid, λ is the wavelength of centre frequency, and $\bar{\sigma}$ and $\bar{\epsilon}$ are the average values of effective conductivity and dielectric constant at centre frequency of the excitation pulse. In addition, a temporal scaling function is modeled to selectively scale reflections from different regions in the reconstruction grid during the two stages of the reconstruction process. A sliding window of variable length is defined based on the residual EM signals, which is used as a temporal scaling function to selectively scale the skin reflections. The temporal scaling functions are applied to a subset of signals that are received by the antennas in the neighbourhood of transmitter, with 90° extension to each side. The scaling functions for the two stages of reconstruction are defined as:

$$\phi_1(m,n,t) = e^{-((t-\zeta_{m,n})/w_1)^2} \quad (11)$$

$$\phi_2(m,n,t) = 1 - e^{-((t-\zeta_{m,n})/w_2)^2} \quad (12)$$

where w_1 and w_2 are the widths of the scaling functions for Stage I and II, respectively. The widths of scaling functions are determined based on the UWB pulse used as excitation signal. $\zeta_{m,n}$ is the location of the sliding window, which is determined by the absolute value of each residual signal corresponding to transmitter m and receiver n at the first step of the iterative inversion algorithm.

Fig. 3 shows the estimation process of the scaling function for a sample residual signal, with $m = 1$ and $n = 4$. The scaling functions are defined at the first step of the iterative process, and used in subsequent iterations for both stages. It is assumed that the measured and estimated signals are calibrated by subtracting the measurements from an empty system scan (without a target); therefore the strongest reflections are rewarded by the weighting function $\phi_1(m, n, t)$ in the first stage (Fig. 3(c)), and suppressed by $\phi_2(m, n, t)$ in the second stage (Fig. 3(d)). The effects of selective scaling and the two stage reconstruction design are described in following section.

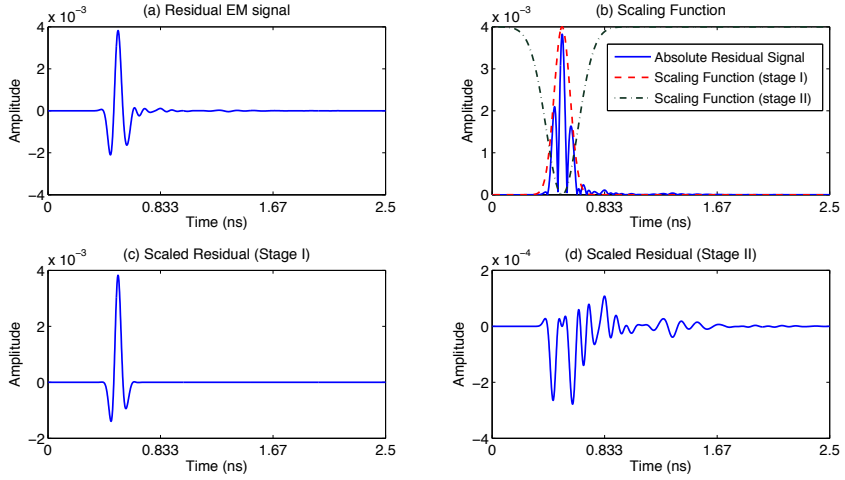

Figure 3: Estimation of scaling function: the absolute value of residual signal is used to estimate the scaling functions for the two stages. (a) Sample residual signal from Channel 1-4 (antenna 1 transmitting and 4 receiving); (b) Plot of absolute residual signal and the estimated scaling functions; (c) Scaled residual signal for stage I; (d) Scaled residual signal for Stage II.

3.2. Multistage Reconstruction

A two stage reconstruction technique is used to initially estimate the skin layer and later reconstruct the dielectric profile of the internal tissue structure.

The residual signals for both stages are calculated as:

$$E^{diff}_{m,n}(t)_j = \phi_j(m,n,t)[E^{meas}_{m,n}(t) - E^{est}_{m,n}(u,t)] \quad , \quad j = 1,2 \qquad (13)$$

The weighting function $\phi_j(m,n,t)$ is chosen for each stage j in the multistage reconstruction process.

3.2.1. Skin Reconstruction

The spatial boundary of the skin layer is estimated by using the temporal weighting function chosen to give a higher weighting to the boundary regions of the target, as described in the preceding section. As a result, the weighted cost functional converges more quickly and the skin region can also be approximated in fewer iterations. The effect of temporal scaling is illustrated in Fig. 4, where the normalized residual error for the scaled (Stage I: green, Stage II: red) and non-scaled (blue) reconstruction is plotted against the number of iterations. The inversion process is terminated once the change in normalized residual error drops below the predefined threshold, and the reconstructed dielectric profile from Stage I is used to construct a skin model by segmenting the skin region using the level-set technique, described in [36]. The Debye model for skin region in the model is estimated by fitting on the skin measurements published in [34].

3.2.2. Reconstruction of Breast Dielectric Profile

In Stage II, the breast dielectric profile is reconstructed using the estimated skin model. The temporal scaling function is chosen to suppress the reflections coming from any mismatch between the actual skin layer and the estimated model. As a result of the suppressed skin reflections, the scattered EM signal from the internal tissue structure now has a larger contribution to the gradients, resulting in a significant improvement in the overall convergence of the inversion algorithm, as shown in Fig. 4. In contrast, the non-scaled standard method (Fig.4: blue) has a slow convergence rate and an inaccurate reconstructed profile. The simplified numerical breast phantom shown in Fig. 2 has been used as

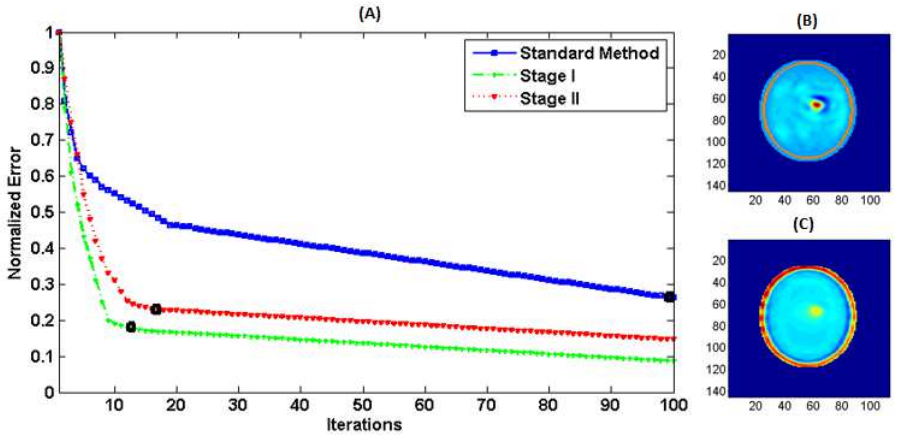

Figure 4: Plots of normalized residual error with standard tomography algorithm (blue) and the proposed method (Stage I: green, Stage II: red) are shown in (A), and the real parts of reconstructed permittivity profiles at 4GHz are shown in (B) and (C). The real part of reconstructed permittivity after 30 iterations of proposed method (Stage I: 12 iterations, and Stage II: 18 iterations) is shown in (B). (C) shows the real part of reconstructed permittivity after 100 iterations of standard method.

a test case for both methods, and the real part of the reconstructed permittivity at 4GHz is shown in the sub-figures Fig. 4(B-C). The real part of reconstructed permittivity after 30 iterations of proposed method (Stage I: 12 iterations, and Stage II: 18 iterations) is shown in (B). (C) shows the real part of reconstructed permittivity after 100 iterations of standard method. It must be noted that the reconstructed permittivity using the multistage approach (Fig. 4: B) has significantly better tumor to background contrast, compared to the standard method. The residual reconstruction error in the multistage technique is much less than the standard approach.

4. Numerical Simulation and Discussion

The proposed multistage technique is verified using set of MRI derived numerical breast phantoms from the UWCEM [23] repository as test cases. The parameters of the Debye models are derived from the data presented in [37]. A modulated Gaussian signal with center frequency of 4GHz and -3dB bandwidth

of 4.5GHz is used as an excitation signal in the Finite Difference Time Domain (FDTD) simulation. A circular array of 18 point sources are modeled in the FDTD simulation as transmitting and receiving antennas with a 0.5mm spatial grid resolution, and the scattered EM signals from the numerical breast phantoms are recorded. In order to avoid the inverse crime, the EM signals from the breast phantom simulation are corrupted with white Gaussian noise to produce a SNR of 40dB, and the FDTD grid resolution is doubled for the measured signals compared to the FDTD solution in reconstruction process. The width of scaling windows w_1 and w_2 for Stage I and Stage II are chosen as 1.1 ns and 2.95 ns, respectively. These values are empirically calculated and represent approximately 1.5 and 4.5 times the pulse width used to illuminate the breast model in simulation. The spatial scaling function γ is calculated using the dielectric values of adipose, where the reference data is derived from [37].

4.1. Skin Reconstruction

A dataset of numerical breast phantoms with different uniform skin thicknesses was created to evaluate the accuracy of the proposed skin estimation method. A 2D slice of Class 1 breast phantom from [23] is used, where the skin layer was artificially varied from 1mm to 4mm in steps of 1mm to create 4 numerical phantoms for the experiment. The structural similarity is very important in the reconstruction of skin geometry; therefore, Structural Similarity Index Metric (SSIM) [38] and Mean Squared Error (MSE) were used as quality assessment metrics for skin reconstruction. The skin models of different uniform thicknesses and the normalized reconstructed profiles are shown in Fig. 5, where A1-A4 are the reference skin models derived from the numerical breast phantom, B1-B4 are the reconstructed profiles, and C1-C4 are the segmented skin regions to be used as starting points for the second stage of reconstruction. The skin layer from the reconstructed profiles is segmented using the shape estimation technique presented in [36]. The structural quality of the reconstructed skin layer is evaluated using binary images of the numerical model and the reconstructed skin, where the skin layer is represented as one and the background

is set to zero. The structural similarity score is found to be more than 0.98 and MSE is less than 0.03 for all of the four breast skin models.

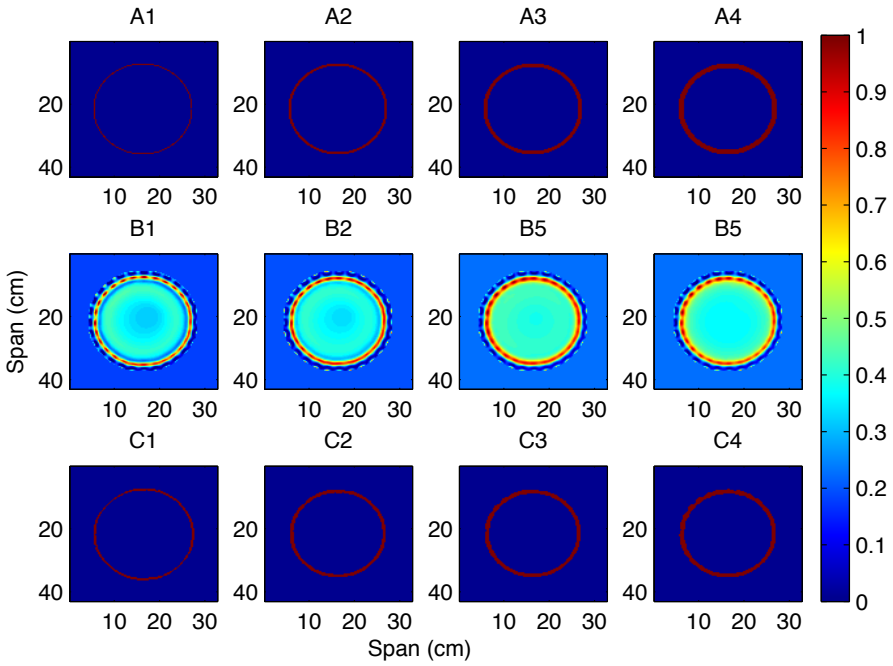

Figure 5: Skin reconstruction: (A1-A4) FDTD models of skin with variations in thickness from 1mm to 4mm in steps of 1mm; (B1-B4) Reconstructed normalized tomography profiles using proposed method in STAGE I; (C1-C4) Segmented skin region from the reconstructed profiles.

4.2. Breast Dielectric Profile Reconstruction

The estimated skin layer from Stage I is used as an initial estimate in Stage II to reconstruct the dielectric properties of the internal tissue structures. The Debye parameters $\epsilon_\infty = 15.9$, $\Delta\epsilon = 23.8$, and $\sigma = 0.83$ are used for the skin region in the initial estimate for Stage II. The skin dielectric values are kept fixed, while the region bounded by the skin layer is updated during the reconstruction process. Fig. 6 shows the real part of permittivity at 4GHz of the numerical breast phantoms of Class 1-3 (A1-A3), and the corresponding reconstructed di-

electric profiles using the standard time domain inversion method (B1-B3) and the proposed multistage method (C1-C3). Although the convergence rate may vary significantly based on the line search method used to find the optimal step size and the problem geometry, a comparison of the convergence of the proposed method and the standard method can be made using the same models and the update procedures. In addition similar termination criteria (See Table 1: step 9) are used for both methods. The average number of iterations for the standard method in reconstructing the three breast phantoms is 120, while the combined iterative steps for the two stages are 35 to produce the results in Fig. 6. It can be seen that the quality of the reconstruction has been significantly improved by incorporating the skin information.

Next, in order to quantitatively compare the quality of reconstructed dielectric profiles, SSIM and Normalized Squared Error (NSE) are calculated for both methods and the results are presented in Fig. 7. The normalized squared error is calculated as:

$$NSE = \frac{1}{3}\sum_{i=1}^{3}\frac{\int_S ||u_i^{actual} - u_i^{reconstructed}||^2}{\int_S ||u_i^{actual}||^2}$$

Where u_i^{actual} and $u_i^{reconstructed}$ are the parameters of Debye model for the breast phantom. In order to present a fare comparison, NSE is calculated only within the interior of the breast excluding the skin region. It can be observed that the NSE is relatively higher (more than 0.2) for both methods, which occurs as a result of the smoothness imposed on the solution through regularization. The distribution of the model dielectric profile has randomness and spatial diversity; therefore, a smooth solution may result in a relatively larger error compared to an unconstrained solution. Using the proposed two stage approach, the normalized reconstruction error has been significantly reduced (average factor of 2), with a reasonably good structural similarity of the solution. The actual skin dielectric properties may vary from patient to patient, causing a mismatch in the skin model for Stage II. In order to study the sensitivity of the solution to a mismatch between the actual dielectric properties of the skin and the properties used to construct the skin model, a mismatch error

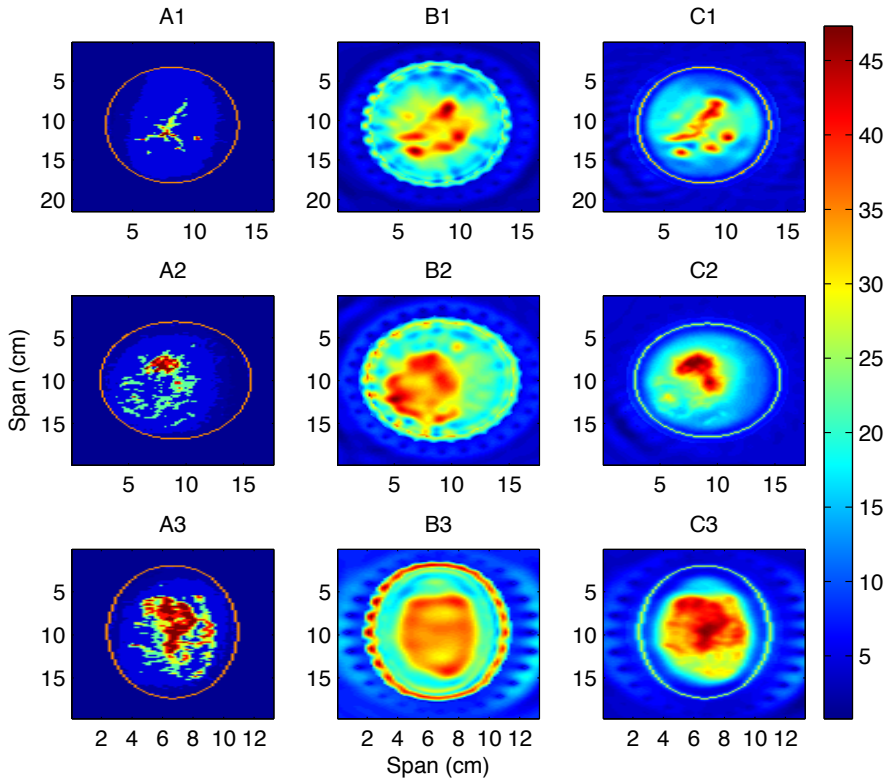

Figure 6: (A1-A3) Real part of permittivty of MRI derived numerical phantoms of class 1-3 at 4GHz; (B1-B3) Real part of the reconstructed permittivity at 4GHz using standard time domain method; (C1-C3) Real part of the reconstructed permittivity at 4GHz using the proposed multistage approach.

in the skin model is introduced and the normalized squared error is shown in Fig. 8. The NSE is plotted against the percentage mismatch error in the skin dielectric properties. It must be noted that at approximately 90% mismatch error, the skin dielectric properties become equal to the adipose dielectric properties, which effectively means that no skin information is used in the second stage. Therefore, the second stage results are almost identical to the standard method.

The percentage mismatch in Fig. 8 is calculated as a percentage of the actual dielectric properties of skin in the numerical breast phantom, which are $\epsilon_\infty = 15.9$, $\Delta\epsilon = 23.8$, and $\sigma = 0.83$. Therefore, a 90% mismatch results in a skin region modeled in the initial estimate with $\epsilon_\infty = 14.3$, $\Delta\epsilon = 21.4$, and $\sigma = 0.75$. The quality of the solution deteriorates with an increase in the mismatch error; however, variations in the skin dielectric properties are expected to be relatively small between patients. In a recent study on the dielectric properties of human skin at 300MHz [39], it is shown that the skin dielectric constant varies between men and women and also within the same sex. However, based on measurements from 30 subjects in each category, it was found that the variation is less than 13% in women and 10% in men. Assuming a maximum variation of 13%, a tolerance range can be defined as shown by the shaded region in Fig. 8. It is observed that the SSIM score is greater than 0.85 for a mismatch less than 13%, and NSE is below 0.25.

5. Conclusion

A multistage selective weighting method for UWB microwave breast tomography has been proposed in this paper. The sensitivity of the microwave inversion algorithm to the high contrast skin-adipose boundary is reduced by introducing a spatio-temporal scaling technique. The spatial scaling coefficients are pre-computed and applied during the calculation of gradients of the EM field at each discretized parameter point. In addition, two temporal scaling functions are derived from the residual signals during the first step of the itera-

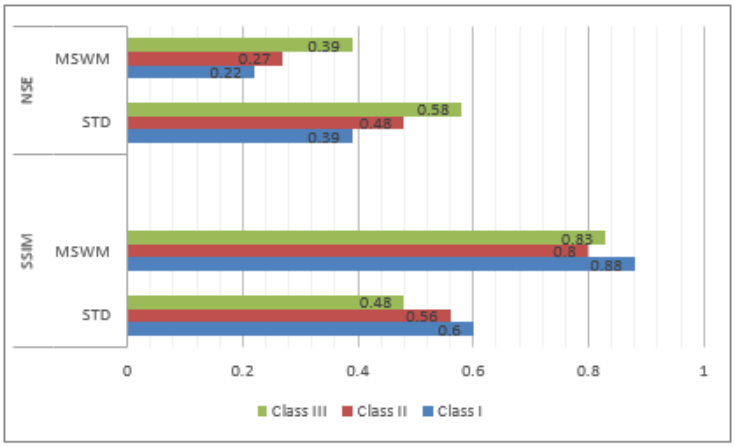

Figure 7: Comparison of reconstruction quality scores (Structural similarity and normalized squared error) for the standard (STD) and multistage (MSWM) method.

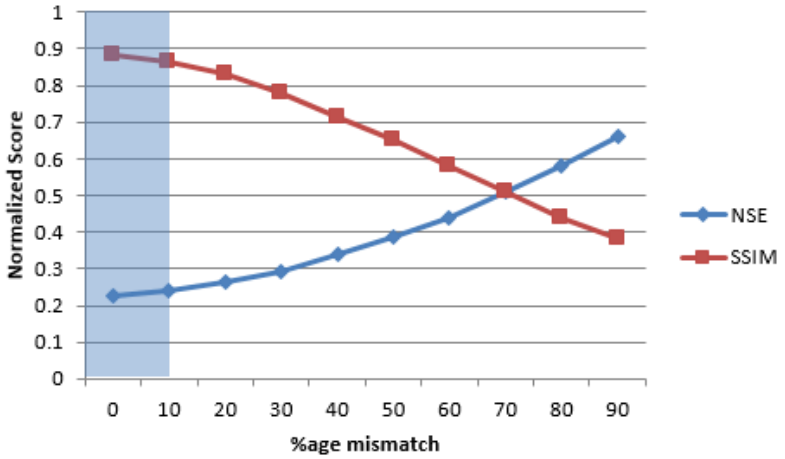

Figure 8: Effect of mismatch in dielectric properties of estimated skin model and the actual breast profile for the STAGE II reconstruction.

tive process and are used to control the sensitivity of the reconstruction to the skin boundary reflections during the two stages of the proposed method. This multistage technique is used to reconstruct 2D slices of MRI derived numerical breast phantoms, and a comparison with the standard non-scaled method shows that the convergence rate has been significantly improved. Moreover, the reconstruction quality of the internal tissue structure of the breast has been notably improved, resulting in a more accurate estimation of the breast tissue structure. The proposed method has been shown to improve the 2D reconstruction, while the reconstruction of 3D breast models will be considered in future studies.

References

[1] S.-H. Son, N. Simonov, H.-J. Kim, J.-M. Lee, S.-I. Jeon, Preclinical prototype development of a microwave tomography system for breast cancer detection, ETRI journal 32 (6) (2010) 901–910.

[2] C. Gilmore, P. Mojabi, A. Zakaria, M. Ostadrahimi, C. Kaye, S. Noghanian, L. Shafai, S. Pistorius, J. LoVetri, A wideband microwave tomography system with a novel frequency selection procedure, Biomedical Engineering, IEEE Transactions on 57 (4) (2010) 894–904.

[3] J. Bourqui, J. Sill, E. Fear, A prototype system for measuring microwave frequency reflections from the breast, International journal of biomedical imaging 2012.

[4] P. M. Meaney, M. W. Fanning, D. Li, S. P. Poplack, K. D. Paulsen, A clinical prototype for active microwave imaging of the breast, Microwave Theory and Techniques, IEEE Transactions on 48 (11) (2000) 1841–1853.

[5] S. C. Hagness, A. Taflove, J. E. Bridges, Two-dimensional fdtd analysis of a pulsed microwave confocal system for breast cancer detection: Fixed-focus and antenna-array sensors, Biomedical Engineering, IEEE Transactions on 45 (12) (1998) 1470–1479.

[6] I. J. Craddock, R. Nilavalan, A. Preece, R. Benjamin, Experimental investigation of real aperture synthetically organised radar for breast cancer detection, in: IEEE AP-S International Symposium, Vol. 1B, Washington, DC, 2005, pp. 179–182.

[7] A. Shahzad, M. O'Halloran, E. Jones, M. Glavin, Pre-filtered beamforming for early stage breast cancer detection.

[8] M. O'Halloran, E. Jones, M. Glavin, Quasi-multistatic mist beamforming for the early detection of breast cancer, Biomedical Engineering, IEEE Transactions on 57 (4) (2010) 830 –840. doi:10.1109/TBME.2009.2016392.

[9] A. E. Bulyshev, S. Y. Semenov, A. E. Souvorov, R. H. Svenson, A. G. Nazarov, Y. E. Sizov, G. P. Tatis, Computational modeling of three-dimensional microwave tomography of breast cancer, IEEE Trans. Microwave Theory Tech. 48 (9) (Sept. 2001) 1053–1056.

[10] T. Takenaka, H. Jia, T. Tanaka, Microwave imaging of electrical property distributions by a forward-backward time-stepping method, Journal of Electromagnetic Waves and Applications 14 (12) (2000) 1609–1626.

[11] P. M. Meaney, K. D. Paulsen, B. W. Pogue, M. Miga, et al., Microwave image reconstruction utilizing log-magnitude and unwrapped phase to improve high-contrast object recovery, Medical Imaging, IEEE Transactions on 20 (2) (2001) 104–116.

[12] D. Kurrant, E. Fear, Regional estimation of the dielectric properties of inhomogeneous objects using near-field reflection data, Inverse Problems 28 (7) (2012) 075001.

[13] R. Scapaticci, I. Catapano, L. Crocco, Wavelet-based adaptive multiresolution inversion for quantitative microwave imaging of breast tissues, Antennas and Propagation, IEEE Transactions on 60 (8) (2012) 3717–3726.

[14] M. Li, O. Semerci, A. Abubakar, A contrast source inversion method in the wavelet domain, Inverse Problems 29 (2) (2013) 025015.

[15] A. Shahzad, M. O'Halloran, M. Glavin, E. Jones, A novel optimized parallelization strategy to accelerate microwave tomography for breast cancer screening, in: Engineering in Medicine and Biology Society (EMBC), 2014 36th Annual International Conference of the IEEE, IEEE, 2014, pp. 2456–2459.

[16] N. Farhat, Microwave holography and coherent tomography, Medical Applications of Microwave Imaging (1986) 66–81.

[17] L. Jofre, M. S. Hawley, A. Broquetas, E. de Los Reyes, M. Ferrando, A. R. Elias-Fuste, Medical imaging with a microwave tomographic scanner, Biomedical Engineering, IEEE Transactions on 37 (3) (1990) 303–312.

[18] G. Peronnet, J. Guerquinkern, M. Gautherie, C. Szeles, Y. Michel, Microwave diffraction tomography for biomedical applications, in: Microwaves & RF, Vol. 22, Penton Publ INC 1100 Superior Ave, Cleveland, OH 44114, 1983, pp. 146–146.

[19] J. C. Bolomey, C. Pichot, G. Garboriaud, Planar microwave imaging camera for biomedical applications: Critical and prospective analysis of reconstruction algorithms, Radio Science 26 (2) (1991) 541–549.

[20] A. Fhager, M. Gustafsson, S. Nordebo, Image reconstruction in microwave tomography using a dielectric debye model, Biomedical Engineering, IEEE Transactions on 59 (1) (2012) 156–166.

[21] M. Lazebnik, L. McCartney, D. Popovic, C. B. Watkins, M. J. Lindstrom, J. Harter, S. Sewall, A. Magliocco, J. H. Booske, M. Okoniewski, et al., A large-scale study of the ultrawideband microwave dielectric properties of normal breast tissue obtained from reduction surgeries, Physics in Medicine and Biology 52 (10) (2007) 2637.

[22] S. Gabriel, R. W. Lau, C. Gabriel, The dielectric properties of biological tissues:III. parametric models for the dielectric spectrum of tissues, Physics in Medicine and Biology 41 (1996) 2271–2293.

[23] E. Zastrow, S. K. Davis, M. Lazebnik, F. Kelcz, B. D. V. Veen, S. C. Hagness, Database of 3d grid-based numerical breast phantoms for use in computational electromagnetics simulations, Online (2008).
URL http://uwcem.ece.wisc.edu/home.htm

[24] T. M. Grzegorczyk, P. M. Meaney, P. A. Kaufman, R. M. di Florio-Alexander, K. D. Paulsen, Fast 3-d tomographic microwave imaging for breast cancer detection, Medical Imaging, IEEE Transactions on 31 (8) (2012) 1584–1592.

[25] J. D. Shea, P. Kosmas, S. C. Hagness, B. D. Van Veen, Three-dimensional microwave imaging of realistic numerical breast phantoms via a multiple-frequency inverse scattering technique, Medical physics 37 (2010) 4210.

[26] Q. Fang, P. M. Meaney, K. D. Paulsen, Microwave image reconstruction of tissue property dispersion characteristics utilizing multiple-frequency information, Microwave Theory and Techniques, IEEE Transactions on 52 (8) (2004) 1866–1875.

[27] D. W. Winters, J. D. Shea, P. Kosmas, B. D. Van Veen, S. C. Hagness, Three-dimensional microwave breast imaging: Dispersive dielectric properties estimation using patient-specific basis functions, Medical Imaging, IEEE Transactions on 28 (7) (2009) 969–981.

[28] A. Fhager, S. Padhi, J. Howard, 3d image reconstruction in microwave tomography using an efficient fdtd model, Antennas and Wireless Propagation Letters, IEEE 8 (2009) 1353–1356.

[29] J. E. Johnson, T. Takenaka, K. Ping, S. Honda, T. Tanaka, Advances in the 3-d forward–backward time-stepping (fbts) inverse scattering technique

for breast cancer detection, Biomedical Engineering, IEEE Transactions on 56 (9) (2009) 2232–2243.

[30] D. R. Gibbins, T. Henriksson, I. Craddock, M. Sarafianou, Time-domain inverse scattering with a coarse reconstruction mesh, in: Microwave Conference Proceedings (APMC), 2011 Asia-Pacific, IEEE, 2011, pp. 485–488.

[31] D. W. Winters, E. J. Bond, B. D. Van Veen, S. C. Hagness, Estimation of the frequency-dependent average dielectric properties of breast tissue using a time-domain inverse scattering technique, Antennas and Propagation, IEEE Transactions on 54 (11) (2006) 3517–3528.

[32] A. Tikhonov, Solutions of ill-posed problems.

[33] B. T. Polyak, The conjugate gradient method in extremal problems, USSR Computational Mathematics and Mathematical Physics 9 (4) (1969) 94–112.

[34] S. Gabriel, R. W. Lau, C. Gabriel, The dielectric properties of biological tissues: II. measurements in the frequency range 10 hz to 20 ghz., Phys Med Biol 41 (11) (1996) 2251–2269.

[35] P. Meaney, S. Pendergrass, M. Fanning, K. Paulsen, Importance of using a reduced contrast coupling medium in 2d microwave breast imaging, Journal of Electromagnetic Waves and Applications 17 (2) (2003) 333–355.

[36] C. Li, C. Xu, C. Gui, M. D. Fox, Distance regularized level set evolution and its application to image segmentation, Image Processing, IEEE Transactions on 19 (12) (2010) 3243–3254.

[37] M. Lazebnik, M. Okoniewski, J. H. Booske, S. C. Hagness, Highly accurate debye models for normal and malignant breast tissue dielectric properties at microwave frequencies, Microwave and Wireless Components Letters, IEEE 17 (12) (2007) 822–824.

[38] Z. Wang, A. C. Bovik, H. R. Sheikh, E. P. Simoncelli, Image quality assessment: from error visibility to structural similarity, IEEE Transactions on Image Processing 13 (4) (2004) 600–612. doi:10.1109/TIP.2003.819861.

[39] H. N. Mayrovitz, S. Carson, M. Luis, Male–female differences in forearm skin tissue dielectric constant, Clinical physiology and functional imaging 30 (5) (2010) 328–332.